Bull. Mater. Sci., Vol. 40, No. 1, February 2017, pp. 45–53. © Indian Academy of Sciences.
DOI 10.1007/s12034-016-1353-1

Synthesis of high-surface-area spinel-type $MgAl_2O_4$ nanoparticles by $[Al(sal)_2(H_2O)_2]_2[Mg(dipic)_2]$ and $[Mg(H_2O)_6][Al(ox)_2(H_2O)_2]_2{\cdot}5H_2O$: influence of inorganic precursor type

ARMAGHAN MIROLIAEE[1], ALIREZA SALEHIRAD[2,*] and ALI REZA REZVANI[1]
[1]Department of Chemistry, University of Sistan and Baluchestan, Zahedan 98135-674, Iran
[2]Institute of Chemical Technologies, Iranian Research Organization for Science and Technology, Tehran 33535-111, Iran

MS received 16 March 2016; accepted 9 June 2016

Abstract. **Spinel-type $MgAl_2O_4$ nanoparticles with high surface area were synthesized by thermal decomposition of three different ion-pair complexes precursors, including $[Mg(H_2O)_6][Al(dipic)_2]_2{\cdot}6H_2O$, $[Al(sal)_2(H_2O)_2]_2[Mg(dipic)_2]$ and $[Mg(H_2O)_6][Al(ox)_2(H_2O)_2]_2{\cdot}5H_2O$. Influence of the inorganic precursor was investigated on synthesis and textural properties of magnesium aluminate nanopowders. The precursors $[Mg(H_2O)_6][Al(dipic)_2]_2{\cdot}6H_2O$ and $[Al(sal)_2(H_2O)_2]_2[Mg(dipic)_2]$ displayed pure spinel-type $MgAl_2O_4$, while the sample synthesized by $[Mg(H_2O)_6][Al(ox)_2(H_2O)_2]_2{\cdot}5H_2O$ precursor consisted of $MgAl_2O_4$ and MgO. The $MgAl_2O_4$ synthesized via $[Al(sal)_2(H_2O)_2]_2[Mg(dipic)_2]$ precursor exhibited higher BET specific surface area (226.7 $m^2\ g^{-1}$) and smaller particle size than those of the samples obtained from the two other precursors.**

Keywords. **Spinel; inorganic precursor; nanoparticles; $MgAl_2O_4$; surface area.**

1. Introduction

Spinel-type magnesium aluminate, $MgAl_2O_4$, is an effective refractory ceramic for metallurgical, cement, chemical, electrochemical and radio technical industries due to its suitable properties, such as good mechanical strength at high temperatures, high resistance to chemical attacks and low thermal conductivity and expansion [1–5].

Several synthetic methods such as gel combustion [6,7], hot pressing [8], mechano-chemical [9], spark plasma sintering [10], molten salt [11], co-precipitation [12], metal–chitosan complexation [13], solution combustion [14], sol–gel auto-combustion [15], sol–gel [16], sonochemical [17], microwave-assisted combustion [18], autoignition [19] and solid-state [20] methods have been used to fabricate $MgAl_2O_4$ spinel powders.

We recently developed a new method for the synthesis of $MgAl_2O_4$ nanoparticle with improved properties, by using an ion-pair complex precursor [21]. In our previous study, advantages of ion-pair complex precursor route based on $[Mg(H_2O)][Al(dipic)_2]_2{\cdot}6H_2O$ (scheme 1) precursor such as creating high BET specific surface area, nano-sized particles and low degree agglomeration were evidenced by comparison with two conventional methods of co-precipitation and sol–gel.

Now, in this research to specify ion-pair complex precursor influence, spinel-type $MgAl_2O_4$ nanoparticles are synthesized by using two other new ion-pair complex precursors, $[Al(sal)_2(H_2O)_2]_2[Mg(dipic)_2]$ (scheme 2) and $[Mg(H_2O)_6][Al(ox)_2(H_2O)_2]_2{\cdot}5H_2O$ (scheme 3), and structural properties of the spinel nanopowders obtained through two different ion-pair complex precursors and the sample synthesized via $[Mg(H_2O)_6][Al(dipic)_2]_2{\cdot}6H_2O$ precursor are compared.

*Author for correspondence (a.r.salehirad@gmail.com, salehirad@irost.ir)

2. Experimental

2.1 *Materials*

The starting chemicals with laboratory grade purity were obtained from Sigma-Aldrich. Procedures of ammonium 2,6-pyridinedicarboxylate and $MgAl_2O_4$ syntheses through $[Mg(H_2O)_6][Al(dipic)_2]_2{\cdot}6H_2O$ precursor were reported in our previous work [21].

2.2 *Synthesis of spinel-type magnesium aluminate samples*

2.2a *$[Al(sal)_2(H_2O)_2]_2[Mg(dipic)_2]$ ion-pair complex precursor approach*: To synthesize $[Al(sal)_2(H_2O)_2]_2[Mg(dipic)_2]$, firstly a mixture of 0.2 M aqueous solution of ammonium 2,6-pyridinedicarboxylate (0.84 g, 4 mmol) and a 0.1 M aqueous solution of $Mg(NO_3)_3{\cdot}6H_2O$ (0.52 g, 2 mmol) was stirred at room temperature for 4 h. Then a mixture of 0.2 M aqueous solution of ammonium salicylate (0.62 g, 4 mmol) and a 0.1 M aqueous solution of $Al(NO_3)_3{\cdot}9H_2O$ (0.75 g, 2 mmol) that had been stirred at room temperature for 4 h was added to the first mixture. The final mixture was stirred at room temperature for 2 h and evaporated in air at ambient temperature for 48 h.

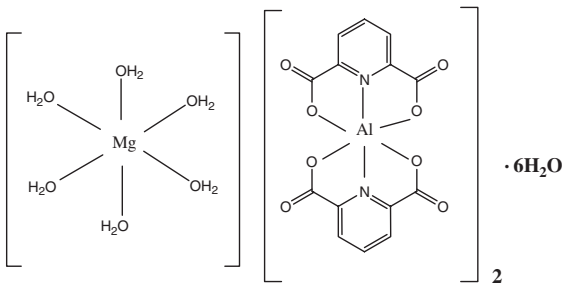

Scheme 1. $[Mg(H_2O)_6][Al(dipic)_2]_2{\cdot}6H_2O$.

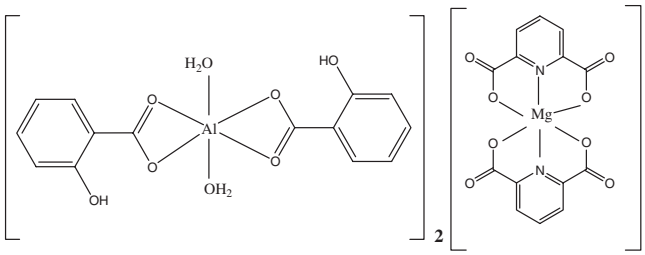

Scheme 2. $[Al(sal)_2(H_2O)_2]_2[Mg(dipic)_2]$.

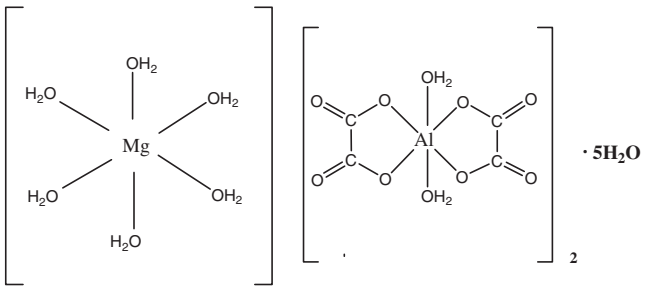

Scheme 3. $[Mg(H_2O)_6][Al(ox)_2(H_2O)_2]_2{\cdot}5H_2O$.

The colourless crystals were collected and dried in air. Anal. Calc. for $C_{42}H_{34}N_2MgAl_2O_{24}$ (M_W = 1028.98 g): C, 49.02; H, 3.33; N, 2.72; found: C, 48.71; H, 3.26; N, 2.56.

For synthesis of $MgAl_2O_4$ spinel, the $[Al(sal)_2(H_2O)_2]_2[Mg(dipic)_2]$ precursor was calcined at 800°C for 4 h.

2.2b *$[Mg(H_2O)_6][Al(ox)_2(H_2O)_2]_2{\cdot}5H_2O$ ion-pair complex precursor approach*: For synthesis of $[Mg(H_2O)_6][Al(ox)_2(H_2O)_2]_2{\cdot}5H_2O$, a 0.2 M aqueous solution of ammonium oxalate (0.50 g, 4 mmol) and a 0.1 M aqueous solution of $Al(NO_3)_3{\cdot}9H_2O$ (0.75 g, 2 mmol) were mixed and stirred at room temperature for 4 h. A 0.05 M aqueous solution of $Mg(NO_3)_2{\cdot}6H_2O$ (0.26 g, 1 mmol) was then added to this mixture. The resulting mixture was stirred at room temperature for 2 h and maintained in air at ambient temperature to evaporate. The colourless crystals were collected and dried in air. Anal. calc. for $C_8H_{30}MgAl_2O_{31}$ (M_W = 700.59 g): C, 13.71; H, 4.32; found: C, 13.59; H, 4.41.

Spinel-type $MgAl_2O_4$ was obtained from calcination of the $[Mg(H_2O)_6][Al(ox)_2(H_2O)_2]_2{\cdot}5H_2O$ complex at 800°C for 4 h.

2.3 *Sample characterization*

Elemental analysis was obtained by a Perkin-Elmer 2400 CHNS/O elemental analyser. The metal contents of precursor were determined by atomic absorption spectroscopy using a Varian AA50 equipment. Conductivity reading was obtained using a Ciba Corning model check-mate 90 conductivity metre. Infrared spectra (4000–400 cm^{-1}) were recorded as KBr discs using a FT-IR PHILIPS, PU9624 spectrophotometer. Electronic spectra were performed on a Perkin-Elmer, Lambda 25 spectrophotometer. Thermal gravimetric analysis (TGA)/differential thermal analysis (DTA) measurements were carried out on an STA503 instrument (BÄHR — Thermoanalyse GmbH, Hüllhorst, Germany) at a heating rate of 10°C min^{-1} over temperature range of 10–900°C, in air atmosphere. XRD patterns were performed on a Inel-3000 diffractometer using Cu Kα (λ = 1.5418 Å) as incident radiation. The BET surface areas and pore volumes of samples were measured with a BELSORB mini-model apparatus. Scanning electron microscopy (SEM) of the samples was investigated using a Zeiss Sigma VP SEM equipped with Oxford EDX/WDX detectors.

3. Results and discussion

3.1 *Ion-pair complex precursor characterization*

The ion-pair complex of $[Al(sal)_2(H_2O)_2]_2[Mg(dipic)_2]$ consists of a cationic part ($[Al(sal)_2(H_2O)_2]^+$) and an anionic part ($[Mg(dipic)_2]^{2-}$). In its cationic part, salicylate as a bidendate ligand is coordinated to the Al through two oxygen atoms of carboxylate and water is also bonded to aluminium through donor oxygen atom, and in its anionic part ($[Mg(dipic)_2]^-$), the dipic anion as a tridendate ligand is coordinated to the Mg via one oxygen of each carboxylate and the nitrogen atom. In the $[Mg(H_2O)_6][Al(ox)_2(H_2O)_2]_2{\cdot}5H_2O$, cationic part, $[Mg(H_2O)_6]^{2+}$, is composed of six aqua ligands and anionic part, $[Al(ox)_2(H_2O)_2]^-$, is composed of two bidendate oxalate ligands ($C_2O_4^{2-}$) and two aqua ligands.

In the infrared spectrum of the $[Al(sal)_2(H_2O)_2]_2[Mg(dipic)_2]$ ion-pair complex (figure 1), there are three sets of absorption bands corresponding to aqua (3500–3000 cm^{-1}, ν(O–H)), salicylate (1560 cm^{-1}, υ_{as}(COO) and 1472 cm^{-1}, υ_s(COO)) and dipic (1618 cm^{-1}, υ_{as}(COO), 1395 cm^{-1}, υ_s(COO), 1252, 1149 and 1038 cm^{-1}, υ(C–O), 908 cm^{-1}, υ(C–COO), and 758 cm^{-1}, δ(COO)) ligands with frequency shift due to coordination. The weak absorption band at about 2400 cm^{-1} is assigned to C–C stretching + (C–H in plane bending/C–N stretching/C–O stretching). The large frequency difference between asymmetric (υ_{as})

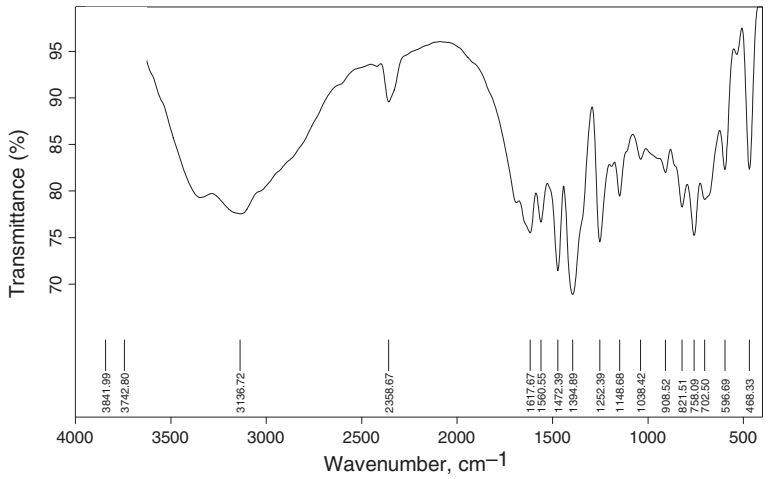

Figure 1. FT-IR spectrum for $[Al(sal)_2(H_2O)_2]_2[Mg(dipic)_2]$.

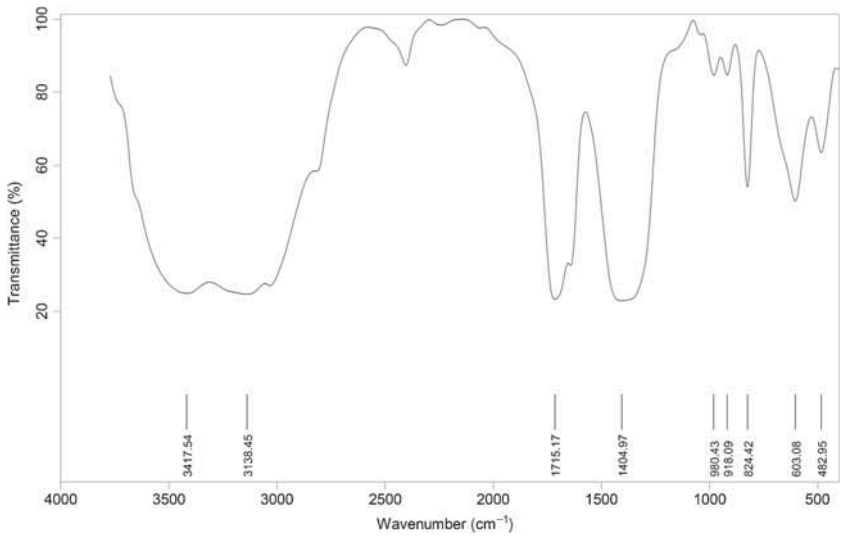

Figure 2. FT-IR spectrum of $[Mg(H_2O)_6][Al(ox)_2(H_2O)_2]_2 \cdot 5H_2O$.

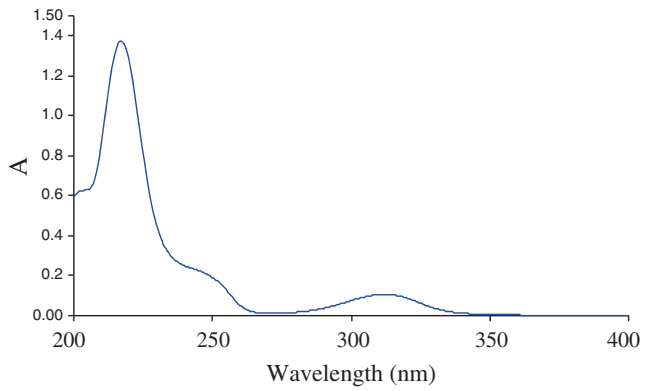

Figure 3. Electronic spectrum of $[Al(sal)_2(H_2O)_2]_2[Mg(dipic)_2]$.

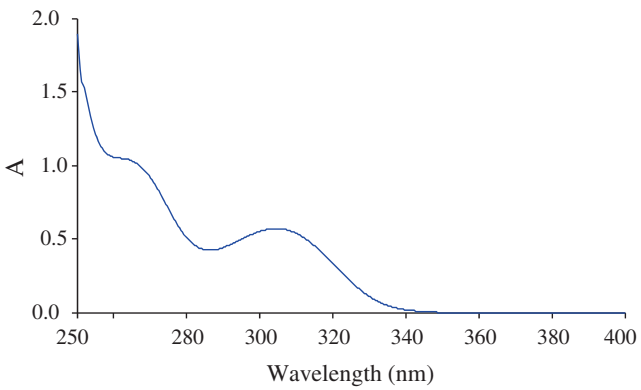

Figure 4. Electronic spectrum of $[Mg(H_2O)_6][Al(ox)_2(H_2O)_2]_2 \cdot 5H_2O$.

and symmetric (υ_s) stretching vibrations of the carboxylate group (223 cm^{-1}) suggests a unidentate coordination of the carboxylate group of dipic to the Mg(II) ion [22]. The absorption bands below 1000 cm^{-1} are due to Mg–O, Mg–N, Al–O_{aqua} and Al–O_{sal} stretching vibrations that indicate the coordination of the ligands to the metals. The FT-IR spectrum of the ion-pair complex, $[Mg(H_2O)_6][Al(ox)_2(H_2O)_2]_2{\cdot}5H_2O$, is illustrated in figure 2. All the vibration modes assigned to both aqua and oxalate (2400 cm^{-1}, υ(C–C) coupled to υ(C–O), 1715 cm^{-1}, υ(C=O), 1405 cm^{-1}, υ(C–O), 980 cm^{-1}, υ(C–C), 918 cm^{-1}, υ(C–COO) and 824 cm^{-1}, δ(COO)) ligands are observed in the FT-IR of the complex. Moreover, absorption modes attributed to stretching vibrations of Mg–O, Al–O_{aqua} and Al–O_{ox} are represented in the 700–400 cm^{-1} region.

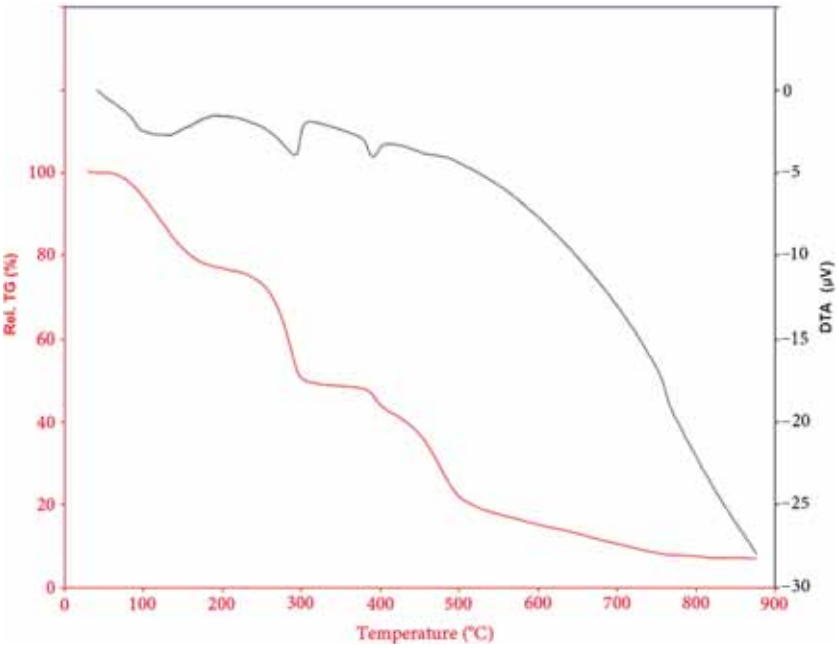

Figure 5. TGA and DTA curves for $[Mg(H_2O)_6][Al(dipic)_2]_2{\cdot}6H_2O$ precursor [21].

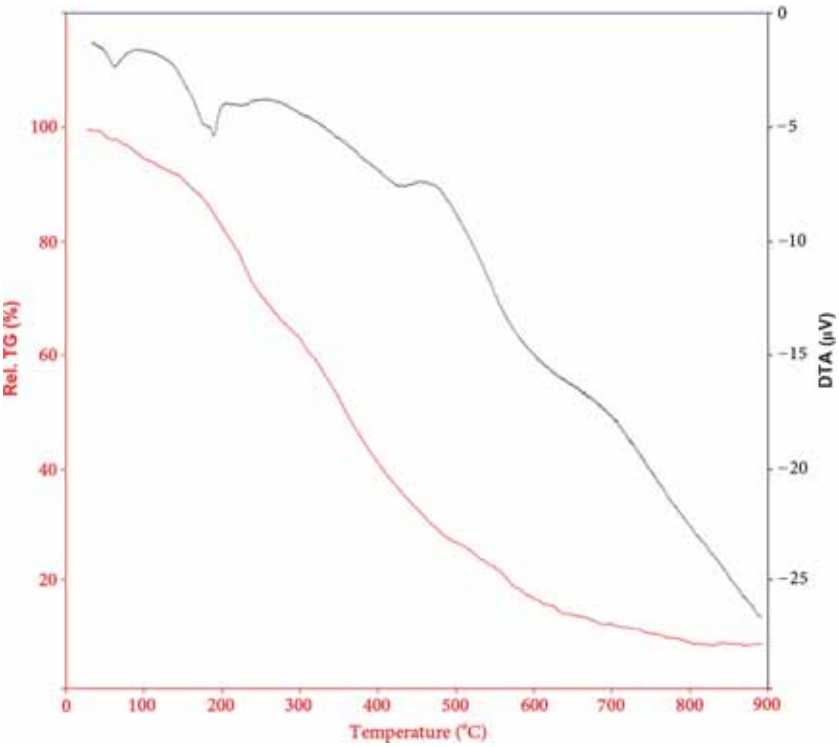

Figure 6. TGA and DTA curves for $[Al(sal)_2(H_2O)_2]_2[Mg(dipic)_2]$ precursor.

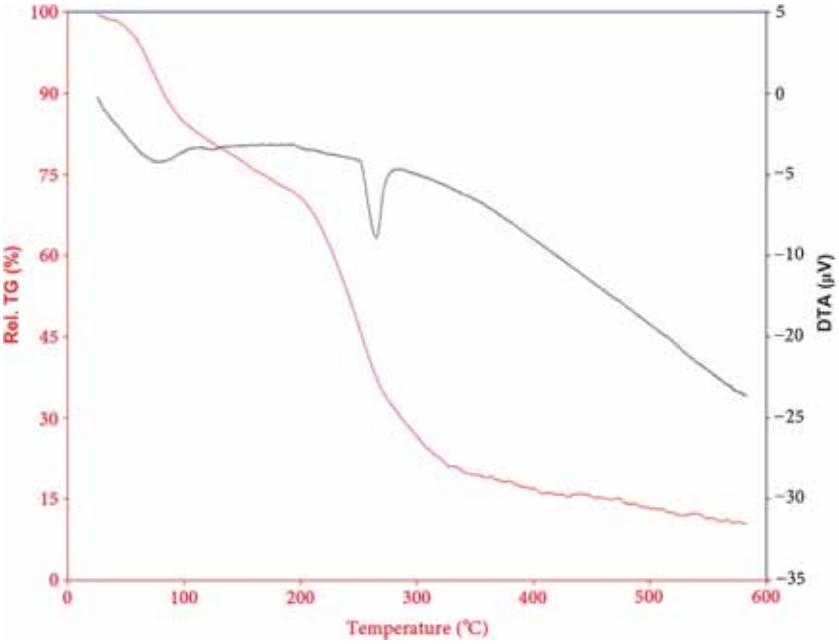

Figure 7. TGA and DTA curves for $[Mg(H_2O)_6][Al(ox)_2(H_2O)_2]_2{\cdot}5H_2O$ precursor.

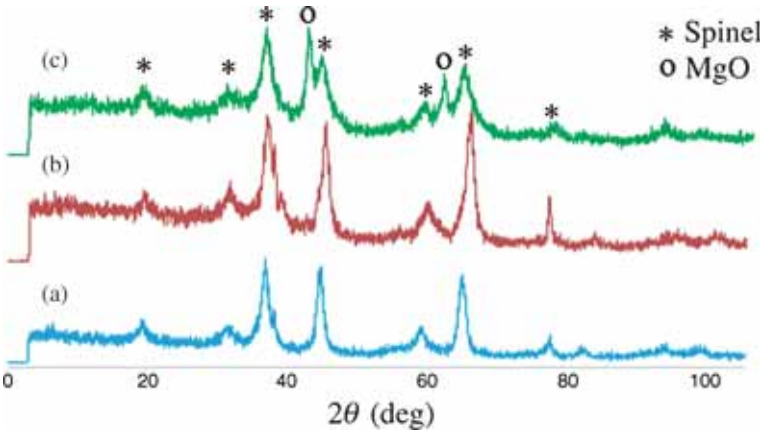

Figure 8. XRD patterns for $MgAl_2O_4$ synthesized by different precursors: (**a**) $[Mg(H_2O)_6][Al(dipic)_2]_2{\cdot}6H_2O$, (**b**) $[Al(sal)_2(H_2O)_2]_2[Mg(dipic)_2]$ and (**c**) $[Mg(H_2O)_6][Al(ox)_2(H_2O)_2]_2{\cdot}5H_2O$.

Table 1. Textural properties of as-synthesized $MgAl_2O_4$ samples.

Ion-pair complex precursor	BET surface area ($m^2\ g^{-1}$)	Crystallite size (nm)
$[Al(sal)_2(H_2O)_2]_2[Mg(dipic)_2]$	226.7	7.4
$[Mg(H_2O)_6][Al(dipic)_2]_2{\cdot}6H_2O$	203.4	8.6
$[Mg(H_2O)_6][Al(ox)_2(H_2O)_2]_2{\cdot}5H_2O$	158.9	6.8 (d_{spinel}), 10.4 (d_{MgO})

The electronic spectrum of the $[Al(sal)_2(H_2O)_2]_2[Mg(dipic)_2]$ complex (figure 3) demonstrates absorption modes at 217, 250 and 311 cm^{-1} corresponding to intraligand and charge transfer transitions In the electronic spectrum of the $[Mg(H_2O)_6][Al(ox)_2(H_2O)_2]_2{\cdot}5H_2O$ complex (figure 4) the absorption bands observed in UV region are due to intraligand and charge transfer transitions. The molar conductivity values for the $[Mg(H_2O)_6][Al(dipic)_2]_2{\cdot}6H_2O$ (275 $ohm^{-1}\ cm^2\ mol^{-1}$), the $[Al(sal)_2(H_2O)_2]_2[Mg(dipic)_2]$ (253 $ohm^{-1}\ cm^2\ mol^{-1}$) and the $[Mg(H_2O)_6]$

$[Al(ox)_2(H_2O)_2]_2{\cdot}5H_2O$ (236 $ohm^{-1}cm^2\ mol^{-1}$) complexes aqueous solutions are in accordance with 1:2 (the first and third) and 2:1 (the second) type electrolytes (three-ion electrolytes).

For investigation of the ion-pair complexes thermolysis, TGA and DTA are carried out from 10 to 900°C at a heating rate of 10°C min^{-1}. The TGA curve (figure 5) shows three weight loss stages for the $[Mg(H_2O)_6][Al(dipic)_2]_2{\cdot}6H_2O$ complex, which are due to the removal of coordinated and crystal water molecules (over 80–160°C) and the decomposition of the four dipic ligands (including two steps in 210–780°C range). The total weight loss and the $MgAl_2O_4$ residue were 91.93% (calcd. 91.80%) and 8.07% (calcd. 8.2%), respectively. In agreement with TGA, the DTA curve exhibits three endothermic processes centred at 150, 340 and 420°C so that the first endothermic process is assigned to the removal of coordinated and uncoordinated water molecules and the two further endothermic processes correspond to the decomposition of the dipic ligands. The TGA diagram (figure 6) displays weight loss stages for the $[Al(sal)_2(H_2O)_2]_2[Mg(dipic)_2]$ complex thermolysis. The first stage over 40–160°C includes about 6.7% weight loss (calcd. 7%) attributed to the loss of coordinated water molecules. The next stage in the 160–800°C region consists of 83.7% weight loss (calcd. 85.4%) corresponding to the removal of the two ligands dipic (two ions) and salicylate (four ions). Finally, the $MgAl_2O_4$ was fagged at about 800°C (obsd. 9.6%, calcd. 7.6%). The DTA curve of the $[Al(sal)_2(H_2O)_2]_2[Mg(dipic)_2]$ complex demonstrates three endothermic processes centred at 70, 190 and 430°C assigned to the removal of coordinated water molecules, 2,6-pyridinedicarboxylate ions and salicylate groups, respectively. The TGA curve for the $[Mg(H_2O)_6][Al(ox)_2(H_2O)_2]_2{\cdot}5H_2O$ complex (figure 7) illustrates two stages of weight loss due to the removal of coordinated and crystal lattice water molecules (over 40–210°C) and oxalate ions (in the temperature range 210–580°C). The total weight loss was 89.1% compared with the calculated value of 88.8% and the residual weight was found to be 10.9% (calcd. 11.2%). The two stages observed in TGA are confirmed by two endothermic peaks centred at 90 and 280°C in DTA curve of the complex attributed to the removal of coordinated and uncoordinated water molecules and the loss of oxalate ligands, respectively.

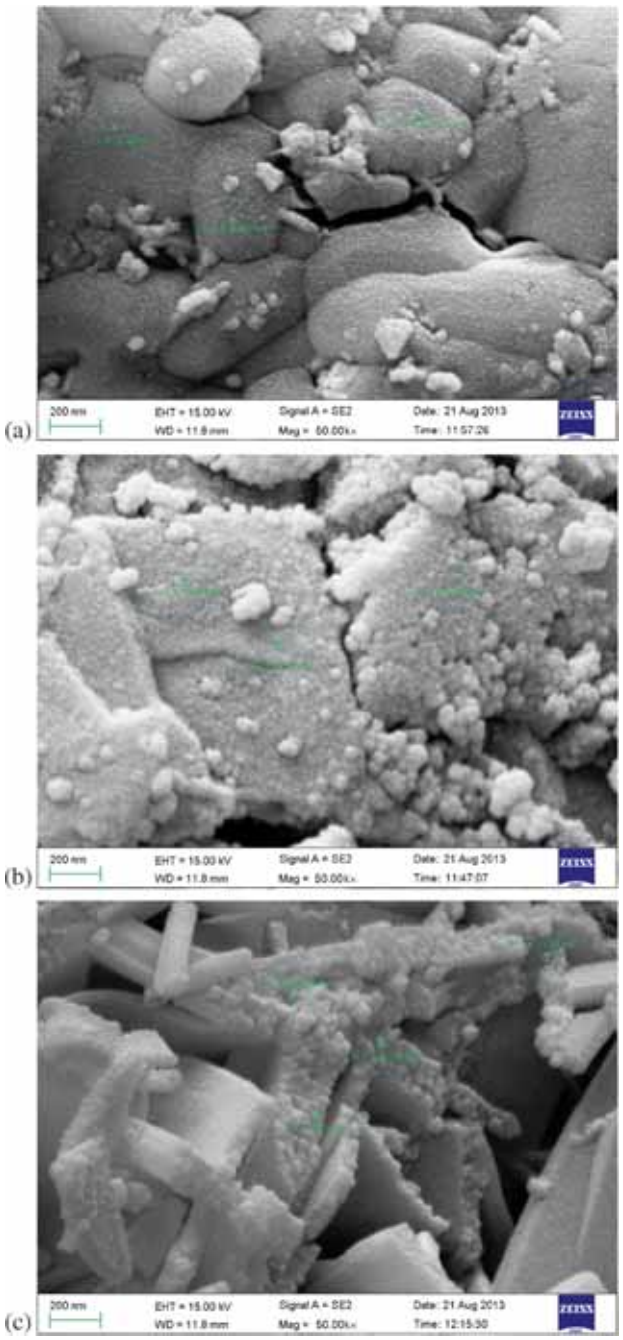

Figure 9. SEM micrographs of samples synthesized through (**a**) $[Al(sal)_2(H_2O)_2]_2[Mg(dipic)_2]$, (**b**) $[Mg(H_2O)_6][Al(dipic)_2]_2{\cdot}6H_2O$ [21] and (**c**) $[Mg(H_2O)_6][Al(ox)_2(H_2O)_2]_2{\cdot}5H_2O$ precursors.

3.2 *Spinel characterization*

Figure 8 presents comparative XRD patterns of the three samples synthesized by different precursors. XRD patterns of both samples synthesized via $[Al(sal)_2(H_2O)_2]_2[Mg(dipic)_2]$ and $[Mg(H_2O)_6][Al(dipic)_2]_2{\cdot}6H_2O$ precursors display pure single phase of $MgAl_2O_4$ spinel in agreement with JCPDS PDF card numbers 089-1627 and 073-2210, respectively, while diffraction peaks in XRD pattern of the sample obtained through $[Mg(H_2O)_6][Al(ox)_2(H_2O)_2]_2{\cdot}5H_2O$ are assigned to two phases of $MgAl_2O_4$ (JCPDS PDF no. 077-0435) and MgO (JCPDS PDF no. 075-1525). Table 1 presents the crystallite sizes of the samples synthesized via different precursors that were measured using the Scherrer relation. As observed from table 1, the $MgAl_2O_4$ spinel synthesized by $[Al(sal)_2(H_2O)_2]_2[Mg(dipic)_2]$ precursor has smaller crystallite size in comparison with the spinel synthesized through $[Mg(H_2O)_6][Al(dipic)_2]_2{\cdot}6H_2O$ precursor.

The comparative investigation of SEM images of the samples synthesized by three different ion-pair complex precursors (figure 9) specifies that both agglomeration degree and particle size are less for the sample synthesized through $[Al(sal)_2(H_2O)_2]_2[Mg(dipic)_2]$ precursor. As

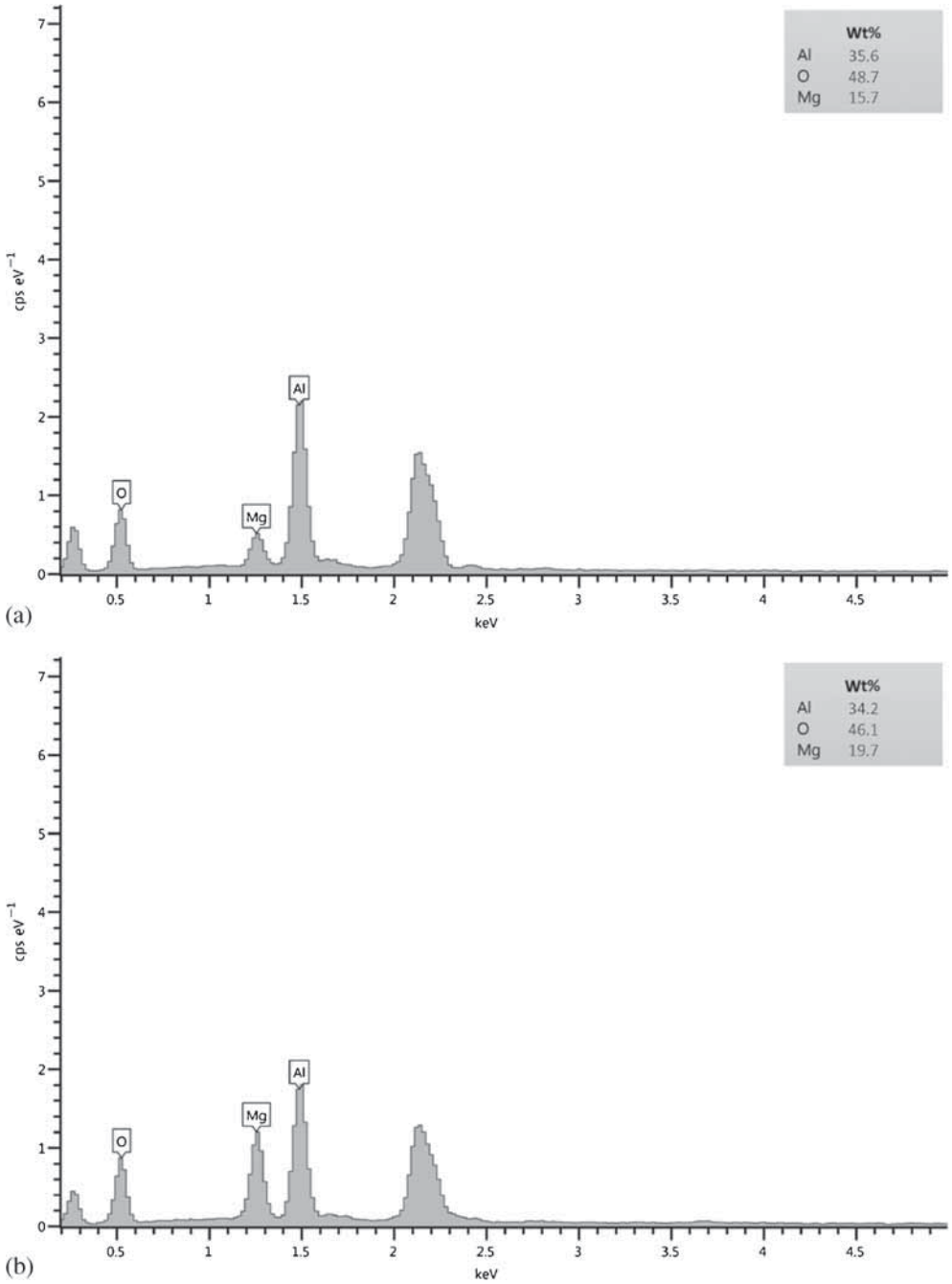

Figure 10. EDX spectra for samples synthesized through (**a**) $[Al(sal)_2(H_2O)_2]_2[Mg(dipic)_2]$ and (**b**) $[Mg(H_2O)_6][Al(ox)_2(H_2O)_2]_2{\cdot}5H_2O$ precursors.

observed from figure 9, SEM image of spinel synthesized by $[Al(sal)_2(H_2O)_2]_2[Mg(dipic)_2]$ precursor displays uniform distinct particles with a narrow size distribution in the range of 13–20 nm, while SEM images for the two other samples (especially for the sample synthesized by the $[Mg(H_2O)_6][Al(ox)_2(H_2O)_2]_2{\cdot}5H_2O$ precursor) exhibit particles that are aggregated and large agglomerates are created. Flake morphology is one of the most common MgO morphologies and can be obtained by different synthesis methods (especially thermal decomposition of coordination compounds method) [23,24]. Therefore, in the SEM image of the sample obtained through the $[Mg(H_2O)_6][Al(ox)_2(H_2O)_2]_2{\cdot}5H_2O$ precursor, existence of flake structure is due to MgO particles and confirms the presence of MgO along with $MgAl_2O_4$ spherical particles.

Figure 10 illustrates EDX spectra for the samples synthesized through $[Al(sal)_2(H_2O)_2]_2[Mg(dipic)_2]$ and $[Mg(H_2O)_6][Al(ox)_2(H_2O)_2]_2{\cdot}5H_2O$ precursors. EDX results confirm formation of pure $MgAl_2O_4$ spinel from $[Al(sal)_2(H_2O)_2]_2[Mg(dipic)_2]$ precursor.

The N_2 adsorption/desorption isotherms for the samples obtained through three different inorganic precursors are

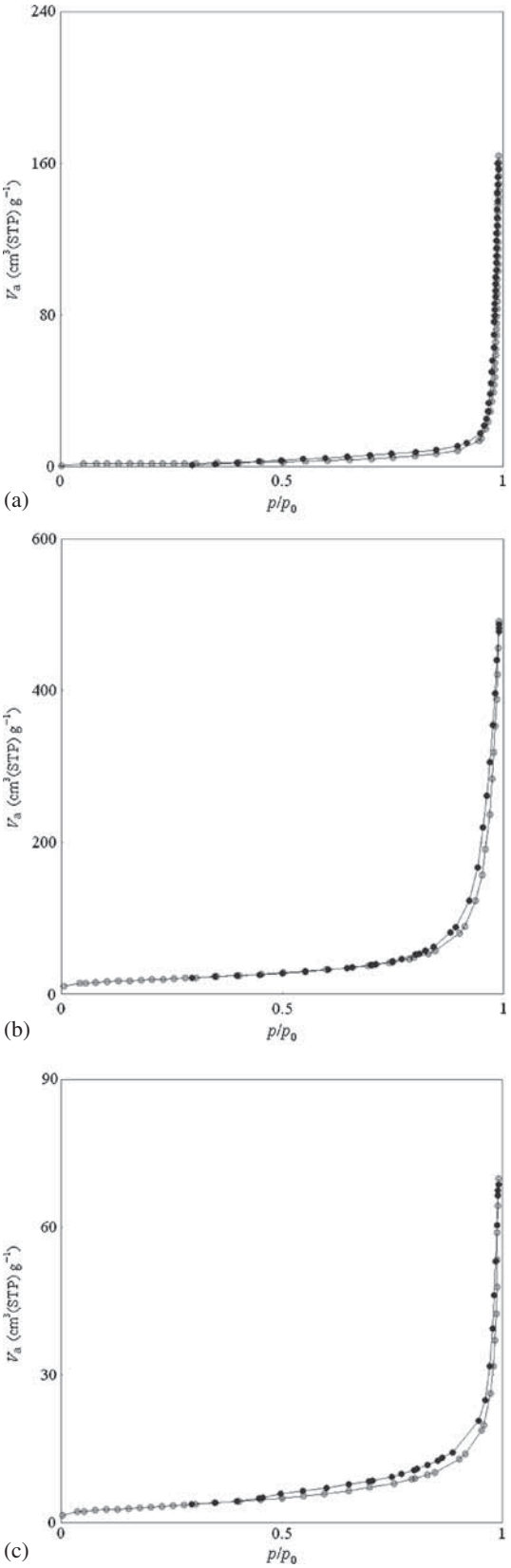

Figure 11. N_2 adsorption/desorption isotherms for samples synthesized via (**a**) $[Mg(H_2O)_6][Al(dipic)_2]_2{\cdot}6H_2O$, (**b**) $[Al(sal)_2(H_2O)_2]_2[Mg(dipic)_2]$ and (**c**) $[Mg(H_2O)_6][Al(ox)_2(H_2O)_2]_2{\cdot}5H_2O$ precursors.

presented in figure 11. All the curves can be considered as a type IV isotherm, typical of mesoporous materials [25].

Comparison of BET surface area values presented in table 1 shows that the sample obtained from $[Al(sal)_2(H_2O)_2]_2[Mg(dipic)_2]$ precursor has the highest BET specific surface area, while the sample synthesized via thermolysis of the $[Mg(H_2O)_6][Al(ox)_2(H_2O)_2]_2{\cdot}5H_2O$ complex exhibits the lowest BET specific surface area, suggesting ion-pair complex precursor influence.

The XRD, SEM and BET results reveal that pure spinel-type $MgAl_2O_4$ is synthesized by $[Al(sal)_2(H_2O)_2]_2[Mg(dipic)_2]$ and $[Mg(H_2O)_6][Al(dipic)_2]_2{\cdot}6H_2O$ precursors as in both of them, the anionic part is a bis(tridendate chelate), while the anionic part of the $[Mg(H_2O)_6][Al(ox)_2(H_2O)_2]_2{\cdot}5H_2O$ complex its composed of more than one ligand type, creating an impure spinel. Moreover, textural properties are the best for the sample synthesized by $[Al(sal)_2(H_2O)_2]_2[Mg(dipic)_2]$ precursor as its cationic part consists of more than one ligand type.

4. Conclusions

Magnesium aluminate nanopowders were synthesized via ion-pair complex precursor route using different precursors such as $[Mg(H_2O)_6][Al(dipic)_2]_2{\cdot}6H_2O$, $[Al(sal)_2(H_2O)_2]_2[Mg(dipic)_2]$ and $[Mg(H_2O)_6][Al(ox)_2(H_2O)_2]_2{\cdot}5H_2O$. Among the precursors, $[Mg(H_2O)_6][Al(dipic)_2]_2{\cdot}6H_2O$ and $[Al(sal)_2(H_2O)_2]_2[Mg(dipic)_2]$ yielded pure single phase of $MgAl_2O_4$ spinel, while $[Mg(H_2O)_6][Al(ox)_2(H_2O)_2]_2{\cdot}5H_2O$ presented $MgAl_2O_4$ along with MgO as impurity. Comparison of textural properties of the samples synthesized by three precursors revealed that the spinel obtained from $[Al(sal)_2(H_2O)_2]_2[Mg(dipic)_2]$ has the highest BET surface area and the smallest particle size.

Acknowledgement

We are grateful to the Iran National Science Foundation and the Iranian Research Organization for Science and Technology for financial support.

References

[1] Jeong N, Yeo J and Song K 2013 *Mater. Lett.* **109** 34
[2] Hashimoto S, Honda S, Hiramatsu T and Iwamoto Y 2013 *Ceram. Int.* **39** 2077
[3] Ganesh I, Reddy G J, Sundararajan G, Olhero S M, Torres P M C and Ferreira J M F 2010 *Ceram. Int.* **36** 473
[4] Salomao R, Villas Bôas M O C and Pandolfelli V C 2011 *Ceram. Int.* **37** 1393
[5] Lavat A E, Grasselli M C and Lovecchio E G 2010 *Ceram. Int.* **36** 15
[6] Padmaraj O, Venkateswarlu M and Satyanarayan N 2015 *Ceram. Int.* **41** 3178
[7] Raj S S, Gupta S K, Grover V, Muthe K P, Natarajan V and Tyagi A K 2015 *J. Mol. Struct.* **1089** 81

[8] Esposito L, Piancastelli A, Miceli P and Martelli S 2015 *J. Eur. Ceram. Soc.* **35** 651

[9] Abdi M S, Ebadzadeh T, Ghaffari A and Feli M 2015 *Adv. Powder Technol.* **26** 175

[10] Fua P, Lua W, Leia W, Xu Y, Wang X and Wu J 2013 *Ceram. Int.* **39** 2481

[11] Zhang D, Li B, Hu Y, Li J and Guo Y 2015 *Ceram. Int.* **41** 5881

[12] Hadian N and Mehran Rezaei 2013 *Fuel* **113** 571

[13] Nuernberg G B, Foletto E L, Probst L F D, Carreño N L V and Moreira M A 2013 *J. Mol. Catal. A Chem.* **370** 22

[14] Lia F, Zhaoa Y, Liua Y, Haoa Y, Liua R and Zhao D 2011 *Chem. Eng. J.* **173** 750

[15] Nassar M Y, Ahmed I S and Samir I 2014 *Spectrochim. Acta Part A Mol. Biomol. Spectrosc.* **131** 329

[16] Liua W, Yang J, Xu H, Wang Y, Hu S and Xue C 2013 *Adv. Powder Technol.* **24** 436

[17] Troia A, Pavese M and Geobaldo F 2009 *Ultrason. Sonochem.* **16** 136

[18] Ganesha I, Johnson R, Rao G V N, Mahajan Y R, Madavendra S S and Reddy B M 2005 *Ceram. Int.* **31** 67

[19] Salem S 2015 *Mater. Chem. Phys.* **155** 59

[20] Sarkar R and Sahoo S 2014 *Ceram. Int.* **40** 16719

[21] Miroliaee A, Salehirad A and Rezvani A R 2015 *Mater. Chem. Phys.* **151** 312

[22] Nakamoto K 2009 *Infrared and Raman spectra of inorganic and coordination compounds*, 6th ed (New York: John Wiley)

[23] Zhang Y, Ma M, Zhang X, Wang B and Liu R 2014 *J. Alloys Compd.* **590** 373

[24] Mageshwari K, Mali S S, Sathyamoorthy R and Patil P S 2013 *Powder Technol.* **249** 456

[25] Zimmermann L M, Almerindo G I, Mora J R, Bechtold I H, Fiedler H D and Nome F 2013 *J. Phys. Chem.* **117** 26097